Letter

# *In situ* generation and manipulation of mirror twin boundaries in transition metal dichalcogenides

Ruo-Han Zhang,[1,3] Jia-Qi He,[1,3] Mo-Han Zhang,[1,3] Ya-Xin Zhao,[1,3] Chao Yan,[1,3] Zi-Han Guo,[1,3] Ya-Ning Ren,[1,3,*] Qi Zheng,[2,†] and Lin He[1,3,‡]

[1]*Center for Advanced Quantum Studies, School of Physics and Astronomy, Beijing Normal University, Beijing 100875, People's Republic of China*

[2]*Department of Applied Physics, School of Physics and Electronics, Hunan University, Changsha 410082, People's Republic of China*

[3]*Key Laboratory of Multiscale Spin Physics, Ministry of Education, Beijing 100875, People's Republic of China*

(Received 18 June 2024; revised 28 July 2024; accepted 13 August 2024; published 26 August 2024)

The mirror twin boundary (MTB) within semiconducting transition metal dichalcogenides (TMDs) not only provides a versatile platform to explore exotic phenomena of one-dimensional (1D) systems, but also offers an effective building block to introduce novel electronic states in the TMDs. In spite of extensive efforts on introducing the MTBs in the TMDs, creating and manipulating the MTBs with custom-designed sites remains an outstanding challenge in experiment. Here we present a facile method for *in situ* generation of MTBs in three different TMDs at predetermined positions by scanning tunneling microscope (STM) tip pulses. In $MoTe_2$, the length and density of the MTBs can be further manipulated using a STM tip. Moreover, we demonstrate the ability to introduce uniform-sized and orderly arranged MTB triangular loops, which generate low-energy flat electronic bands in the $MoTe_2$. A periodic modulation in the density of states with a $3a$ period ($a$ is the lattice constant) is observed in the MTBs. Unexpectedly, our experiment indicates that the MTBs exhibit length preference with $3Na$ ($N$ is an integer), implying that the mechanism for the periodic modulation in the density of states also plays a role in affecting the formation of the MTBs.

DOI: 10.1103/PhysRevB.110.L081407

## I. INTRODUCTION

In one-dimensional (1D) systems, reduced screening, enhanced quantum fluctuation, and confinement effects make them paradigmatic platforms for exploring exotic correlated phenomena, such as quantum spin liquids [1–4], Tomonaga-Luttinger liquid (TLL) [5–8], and Peierls-type charge density wave (CDW) [9–12]. Recently, metallic mirror twin boundary (MTB) within transition metal dichalcogenides (TMDs) has emerged as an ideal candidate for investigating correlated physics in 1D systems due to its embedded nature within the bulk insulating matrix [12–27]. Therefore, researchers have made extensive efforts to synthesize MTBs in the TMDs, such as introducing Mo enrichment by electron beam damage [19,22] and thermal sublimation of chalcogens under vacuum annealing [25]. However, the defect nature of the MTBs makes the creation and manipulation of the MTBs with custom-designed sites a big experimental challenge. The ability to *in situ* generation and manipulation of MTBs is highly demanded, as it is crucial for fundamental understanding and regulating of properties of both the MTBs and TMDs.

In this Letter, we take advantage of the capability atomic-resolution imaging and precise positioning by scanning tunneling microscope (STM) [28–32] and report a facile method of generating and manipulating MTBs of three different TMDs, i.e., $MoTe_2$, $MoSe_2$, and $WSe_2$, at selected positions. By using voltage pulses applied through the tip of a STM, we not only create the MTBs with tunable sizes and densities, but we also can generate uniform-sized and orderly arranged MTB triangular loops with low-energy flat electronic bands. The *in situ* acquisition and manipulation of the MTBs provide us a unique platform to explore exotic electronic states in the TMDs [33,34]. Moreover, the electronic properties of the MTBs with different lengths in $MoTe_2$ were measured, revealing the modulation in the density of states with a $3a$ period ($a = 3.52$ Å is the lattice constant of $MoTe_2$). Unexpectedly, our STM measurement indicates that the MTBs exhibit length preference with $3Na$ ($N$ is an integer), implying that the mechanism for the periodic modulation in the density of states also plays a role in affecting the formation of the MTBs.

## II. *IN SITU* GENERATION AND MANIPULATION OF MTBs

### A. *In situ* generation of MTBs with different lengths

Our measurements were performed on TMDs as well as van der Waals heterostructures made of monolayer graphene stacked on top of the TMDs ($MoTe_2$, $MoSe_2$, and $WSe_2$; see Supplemental Material Figs. S1 and S2 for details [35]). Figure 1(a) schematically illustrates the process to create and manipulate MTBs in the TMDs. Besides the capability of atomic-resolution imaging, the STM has demonstrated the ability to modify the structure of the studied systems locally [28–32]. Here we use STM tip pulses to break the ionic bonds

*Contact author: yning@mail.bnu.edu.cn
†Contact author: zhengqi@hnu.edu.cn
‡Contact author: helin@bnu.edu.cn

 

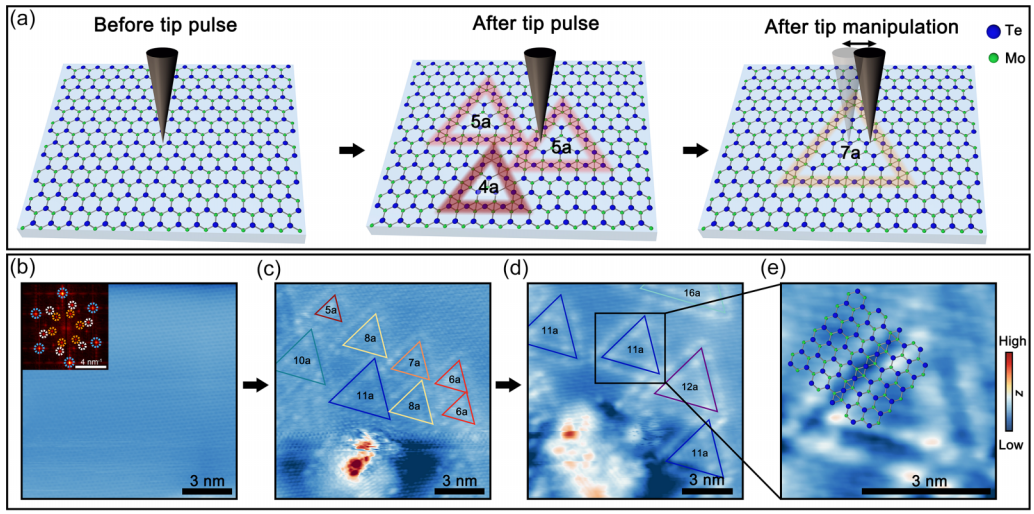


FIG. 1. Schematic illustration and high-resolution STM image of the *in situ* generation and manipulation of MTBs. (a) A schematic model for the formation and further manipulation of MTBs. MTBs of various lengths can be generated through the application of a STM tip pulse and may subsequently be merged into a larger domain with additional tip manipulation (STM tip pulse or quick scanning). The blue and green spheres represent Te atoms and Mo atoms, respectively. The triangles in different colors represent different sizes of MTBs, with *Na* used to label the length of the domain edges, where $a = 3.52$Å is the lattice constant of $MoTe_2$. (b) A representative STM image of graphene/$MoTe_2$ heterostructure. Inset: FFT image obtained from the STM image. The bright spots represent the reciprocal lattice of graphene (blue dotted circles), $MoTe_2$ (white dotted circles), and the moiré structure of the graphene/$MoTe_2$ heterostructure (orange dotted circles) respectively. (c) MTBs of different lengths are created by applying a STM tip pulse. (d) MTBs in panel (c) are merged into larger ones under additional tip manipulation. (e) An enlarged view of the black rectangle in panel (d) corresponds inverse FFT image obtained by filtering the components of graphene. The atomic lattices of $MoTe_2$ are overlaid onto the image.

in TMDs to introduce high density atomic defects (see Supplemental Material Fig. S3 for detailed pulse parameters [35]). As demonstrated previously [19–23], the introduced atomic defects allow for either the metal or chalcogen sublattice to smoothly glide within a triangular area, thereby providing sufficient freedom for the formation of MTBs. By further employing STM tip manipulation techniques, atomic redistribution can be achieved, enabling the merging of several small MTBs into a larger one, as schematically illustrated in Fig. 1(a).

Here, we used the result obtained in the $MoTe_2$ and graphene/$MoTe_2$ heterostructures as examples due to the low barrier for forming high density of MTBs in the $MoTe_2$ [21]. It is worth stating that the monolayer graphene, serving as an atomic-scale protective layer and possessing high chemical stability, not only prevents the semiconductor surface from oxidation but also protects tips against adsorption of other atoms during the tip pulse process. Moreover, experimental results indicate that whether graphene is covered or not has no significant impact on the main conclusions of this study (see the Supplemental Material [35] for details). Figures 1(b)–1(d) summarize the representative process of creating and manipulating the MTBs. Figure 1(b) presents the pristine surface with no atomic defects or strain on graphene/$MoTe_2$ heterostructure and the inset shows the corresponding fast Fourier transform (FFT) image. By using STM tip pulses at a predetermined site of the heterostructure, the topmost graphene monolayer remains intact, however, nanoscale pits can be observed in the TMD substrates [Figure 1(c) and Supplemental Material Fig. S4 [35]). Te vacancies and the MTBs can be observed around the nanoscale pits after the tip pulses (see Supplemental Material Figs. S4 and S5 [35]), implying that the vacancies play an important role in the formation of the MTBs [20–22]. Around the pits, triangle MTBs of different sizes are clearly observed. A close-up view of the MTB is characterized in the high-resolution topography images, as shown in Fig. 1(e). In the $MoTe_2$, the 4|4*P*-type MTB has the lowest formation energy [20], therefore it is the most commonly observed in our experiment. The formation of MTBs is closely related to tip-induced nanopits and atomic defects (see Supplemental Material Fig. S5 for STM characterizations of Te vacancies around the MTBs [35]). High density MTBs are observed around the nanoscale pits, indicating that the boundary of the pits introduces high density chalcogen defects to generate the MTBs. Next, with continued application of the tip pulse, several small MTB domains can aggregate into larger MTB domains, as shown in Figs. 1(c) and 1(d). It implies that further STM tip manipulation can generate more Te vacancies, resulting in the rearrangement of the MTB loops [19]. These experimental phenomena further confirm that the Te vacancies play a crucial role in the formation of MTBs within TMDs (see Supplemental Material Figs. S6 and S7 for more experimental results on the manipulation of other TMDs [35]). Our result demonstrates that MTBs can be generated at selected positions, which offers exciting possibilities for exploring and tuning their properties.

### B. *In situ* generation of periodic MTB superstructures

More interestingly, we demonstrate that our method enables the *in situ* generation of uniform-sized, periodically arranged MTB superstructures in the TMDs. Figure 2(a) shows a typical STM topographic image of an area after applying tip pulses directly onto a graphene/$MoTe_2$

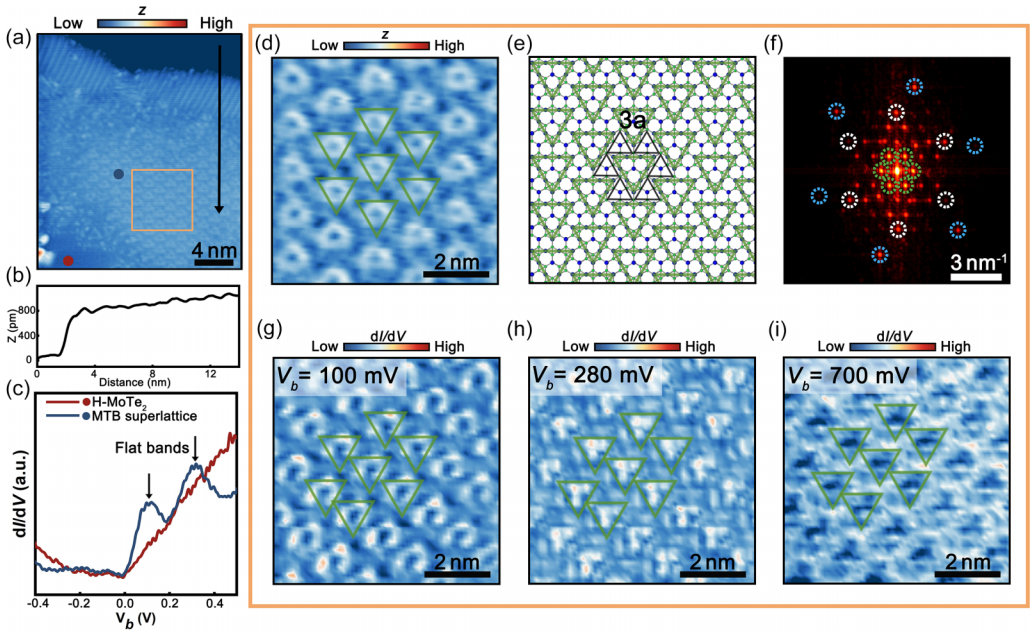


FIG. 2. MTB superlattice and its electronic properties. (a) Uniform-sized and orderly arranged MTBs are created by applying a STM tip pulse ($V_b = 300$ mV, $I = 125$ pA). (b) The height profile along the black arrow in panel (a), showing a nano pit around the MTBs. (c) Typical *dI*/*dV* spectra taken on the *H*-phase $MoTe_2$ and MTB superlattice, respectively. The sample is covered with a monolayer graphene, providing a protection layer in the STM measurement. (d) Magnified STM topographic image within orange square in panel (a), showing the uniformly ordered MTB superlattice. (e) Structural model framed in orange square of panel (a). The black solid line represents the formed coloring-triangle (CT) lattice in the MTB superlattice. (f) Corresponding FFT image of panel (d). The bright spots represent the reciprocal lattice of graphene (blue dotted circles), $MoTe_2$ (white dotted circles), and the MTB supercell (green dotted circles). (g)–(i) The *dI*/*dV* maps of panel (d) acquired at 100 mV (g), 280 mV (h), and 700 mV (i), respectively.

heterostructure. Besides the region showing the MTBs with different lengths, a region with uniform-sized and orderly arranged MTBs can be clearly observed. The magnified STM image, as shown in Fig. 2(d), displays the tip-induced ordered phase, which is distinctly different from the *H*-phase $MoTe_2$ or isolated MTBs. A structural model of the ordered superstructure phase with a lattice constant of 12.2 Å is depicted in Fig. 2(e). The Te atoms on the MTB form closed triangular loops together with the Mo terminated triangular domain of pristine *H*-phase $MoTe_2$. The ordered MTBs form a polymorphic $MoTe_2$ phase, which shares the identical geometry and chemical ratio with the recently found $Mo_5Te_8$ [40]. We emphasize that the MTB superstructures are not quite suitable for studying TLL or CDW physics because of their small size and high density. However, the orderly arranged MTB triangular loops provide a different route to tune electronic properties of the TMD, which enables the realization of exotic quantum phases beyond the parent materials. Scanning tunneling spectroscopy (STS) spectra were acquired in order to characterize the electronic properties of the ordered MTBs [Fig. 2(c)]. The *dI*/*dV* spectrum (orange) acquired on $Mo_5Te_8$ shows two pronounced peaks (0.1 and 0.28 V) near the Fermi level, which are the two low-energy flat electronic bands in the coloring-triangle lattice [34]. Representative spatial-resolved local density of state (LDOS) maps of $Mo_5Te_8$ are shown in Figs. 2(g)–2(i), in line with that reported in a previous study [34]. Obviously, the periodic MTB structure strongly modifies the electronic properties of the TMD. The tip-induced uniform-sized and orderly arranged MTB superlattice provides a unique platform to expand the family of polymorphs of the TMDs, which sequentially can assist us in exploring their exotic electronic states and correlated states.

## III. CHARGE DENSITY MODULATION ALONG THE MTB

The MTBs of varying length and density obtained in our experiments provide a unique platform to explore exotic electronic states in 1D electron systems. Figure 3 illustrates the morphology and electronic structures of various MTB triangular domains with different sizes in the $MoTe_2$. The triangular domains confine the electron within the boundaries. Along the 1D boundaries, i.e., the MTBs, two parallel rows of prominent protrusions are observed, as shown in Fig. 3(a). At a low sample bias ($V_b = 350$ mV), the protrusions exhibit a period of approximately $3a$ along the MTBs, independent of their length. However, the $3a$ periodic modulation is hard to observed when we measure the STM image at a high energy bias (see Fig. S8 for more STM images with other sample bias [35]). Such a result indicates that the periodic modulation in the STM image mainly originates from charge density [12], but whether it is the CDW order or a TLL behavior remains controversial. Recent experimental results suggest that the MTBs embedded in $MoSe_2$ exhibit TLL behavior [8], but this phenomenon has not yet been observed in $MoTe_2$. To further confirm the physical origin of the $3a$ periodic modulation observed in our experiment, we performed STS measurements, as shown in Figs. 3(b) and 3(c). Unlike a typical U-shaped spectrum with a large semiconducting band gap of the pristine $MoTe_2$, the spectrum of MTB displays several peaks within

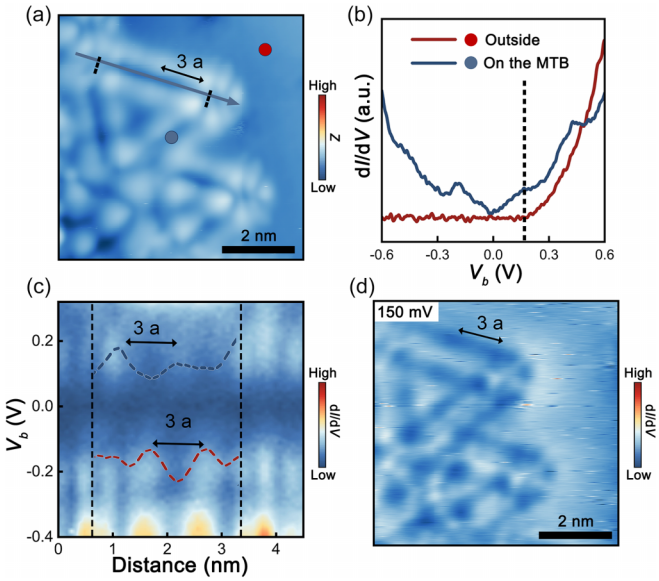


FIG. 3. Charge density modulations of 1D MTB in $MoTe_2$. (a) STM image ($V_b = 350$ mV, $I = 90$ pA) showing the MTBs in $MoTe_2$. (b) Typical STM *dI*/*dV* spectra obtained from pristine few-layer $MoTe_2$ [red dot in panel (a)] and an MTB [blue dot in panel (a)], revealing their semiconducting and metallic characteristics, respectively. (c) Spatially resolved STS spectra of an MTB along the direction of blue arrow in panel (a), uncovering a 3*a*-fold charge modulation. The charge intensity reversal between the occupied (red) and empty (blue) states. (d) Representative *dI*/*dV* constant-height conductance map recorded at $E = 150$ meV, showing the modulation of electronic states along the MTB with a wavelength of 3*a*.

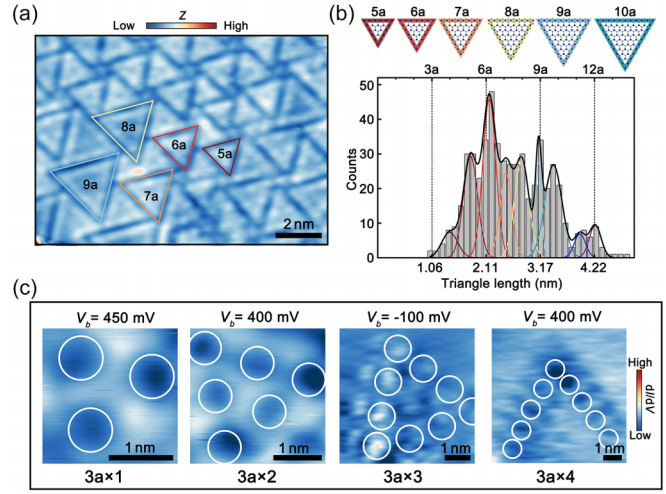


FIG. 4. Histogram of the MTBs showing the existence of length preference. (a) STM image depicting MTBs of varying lengths induced by STM tip pulse. The triangles in different colors represent different sizes of MTBs, where *a* is the lattice constant of $MoTe_2$. (b) Top panel: Illustration of the atomic models for MTB triangles of different sizes. Bottom panel: Statistical analysis of the $MoTe_2$ triangle domain sizes. The colored curves depict the fitting of experimental data, while the black line represents the overall fitting results. The results indicate length preference of the MTBs with lengths as multiples of 3*a*. (c) Representative *dI*/*dV* constant-height conductance maps of the MTBs with an integer multiple length of 3*a*.

the semiconducting gap of the pristine $MoTe_2$. Our *dI*/*dV* spectroscopic map along the MTB, as shown in Fig. 3(c), and energy-fixed STS map, as shown in Fig. 3(d), reveal that the peaks in the tunneling spectra exhibit the same 3*a* period (see Figs. S9–S11 for more data [35]). Although our experiment is measured at 77 K, we still can measure the spatial distributions of the highest occupied states (red dashed line) and the lowest unoccupied states (blue dashed line), which are spatially out of phase [Fig. 3(c)].

## IV. "MAGIC LENGTH" IN MTBs

In our experiment, we cannot precisely control the length of the tip-induced MTBs and the MTBs exhibit a wide length distribution, as shown in Fig. 4(a) as an example. However, the length of the MTBs obtained in our work is not random and seems to exhibit length preference. To clearly show this, we summarized the histogram for the studied MTBs as a function of the length in Fig. 4(b). The length of the MTBs obtained in our experiment is mainly ranging $3a - 13a$ and the numbers exhibit local maxima at 3*a*, 6*a*, 9*a*, and 12*a*, indicating length preference of the MTBs. It implies that the MTBs with these lengths may be considered as "magic length," i.e., the stability of the MTBs is enhanced at these lengths. Such a feature reminds us of the "magic numbers," that atomic clusters with certain numbers of atoms or molecules are particularly stable, resulting from closed electronic shell structure [41–46].

Our experiment indicates that the stability of the MTBs is enhanced when the length is an integer multiple of the period 3*a*, as shown in Fig. 4(c), which reveals a deep connection between the magic length and the observed charge density modulations. It implies that the mechanism that leads to the charge density modulations in the MTBs also plays a role in affecting the structure of the MTBs, i.e., significantly enhancing the stability at specific lengths. In our experiment, we also can frequently observe the MTBs with their length not equal to 3*Na*, implying that the energy difference between the MTBs with and not with the 3*Na* period is quite subtle, which poses significant challenges for exactly considering in theory. In future studies, more theoretical and experimental work are necessary to fully ascertain the exact origin of the magic length in the MTBs.

## V. CONCLUSION

In summary, we report a facile method of generating and manipulating MTBs in three TMDs, i.e., $MoTe_2$, $MoSe_2$, and $WSe_2$, at selected positions. By using STM tip pulses, we not only create the MTBs with tunable sizes and densities, but also generate uniform-sized and orderly arranged MTB triangular loops with low-energy flat electronic bands. In the $MoTe_2$, our STM measurements indicate that the MTBs exhibit charge density modulations with a 3*a* period and show a length preference with 3*Na*.

## ACKNOWLEDGMENTS

This work was supported by the National Key R and D Program of China (Grants No. 2021YFA1400100 and No. 2021YFA1401900), National Natural Science Foundation of China (Grants No. 12141401, No. 12425405, and No. 12404198), "the Fundamental Research Funds for the Central Universities" (Grant No. 310400209521), the China National Postdoctoral Program for Innovative Talents (Grant No. BX20240040), and the China Postdoctoral Science Foundation (Grant No. 2023M740296).



[1] P. W. Anderson, Resonating valence bonds: A new kind of insulator? Mater. Res. Bull. **8**, 153 (1973).

[2] B. J. Kim, H. Koh, E. Rotenberg, S.-J. Oh, H. Eisaki, N. Motoyama, S. Uchida, T. Tohyam, S. Maekawa, Z.-X. Shen, and C. Kim, Distinct spinon and holon dispersions in photoemission spectral functions from one-dimensional $SrCuO_2$, Nat. Phys. **2**, 397 (2006).

[3] B. Lake, D. A. Tennant, C. D. Frost, and S. E. Nagler, Quantum criticality and universal scaling of a quantum antiferromagnet, Nat. Mater. **4**, 329 (2005).

[4] C. Broholm, R. J. Cava, S. A. Kivelson, D. G. Nocera, M. R. Norman, and T. Senthil, Quantum spin liquids, Science. **367**, eaay0668 (2020).

[5] S. Tomonaga, Remarks on Bloch's method of sound waves applied to many-fermion problems, Prog. Theor. Phys. **5**, 544 (1950).

[6] J. M. Luttinger, An exactly soluble model of a many-fermion system, J. Math. Phys. **4**, 1154 (2004).

[7] F. D. M. Haldane, Luttinger liquid theory" of one-dimensional quantum fluids. I. Properties of the Luttinger model and their extension to the general 1D interacting spinless Fermi gas, J. Phys. C: Solid State Phys. **14**, 2585 (1981).

[8] T. Zhu, W. Ruan, Y.-Q. Wang, H.-Z. Tsai, S. Wang, C. Zhang, T. Wang, F. Liou, K. Watanabe, T. Taniguchi, J. B. Neaton, A. Weber-Bargioni, A. Zettl, Z. Q. Qiu, G. Zhang, F. Wang, J. E. Moore, and M. F. Crommie, Imaging gate-tunable tomonaga–luttinger liquids in 1H-$MoSe_2$ mirror twin boundaries, Nat. Mater. **21**, 748 (2022).

[9] G. Grüner, The dynamics of charge-density waves, Rev. Mod. Phys. **60**, 1129 (1988).

[10] R. E. Peierls, *Quantum Theory of Solids* (Oxford University Press, New York, London, 1955).

[11] X. Yang, J.-J. Xian, G. Li, N. Nagaosa, W.-H. Zhang, L. Qin, Z.-M. Zhang, J.-T. Lü, and Y.-S. Fu, Possible phason-polaron effect on purely one-dimensional charge order of $Mo_6Se_6$ nanowires, Phys. Rev. X **10**, 031061 (2020).

[12] L. Wang, Y. Wu, Y. Yu, A. Chen, H. Li, W. Ren, S. Lu, S. Ding, H. Yang, Q.-K. Xue, F.-S. Li, and G. Wang, Direct observation of one-dimensional Peierls-type charge density wave in twin boundaries of monolayer $MoTe_2$, ACS Nano **14**, 8299 (2020).

[13] A. M. van der Zande, P. Y. Huang, D. A. Chenet, T. C. Berkelbach, Y. You, G.-H. Lee, T. F. Heinz, D. R. Reichman, D. A. Muller, and J. C. Hone, Grains and grain boundaries in highly crystalline monolayer molybdenum disulphide, Nat. Mater. **12**, 554 (2013).

[14] X. Zou, Y. Liu, and B. I. Yakobson, Predicting dislocations and grain boundaries in two-dimensional metal-disulfides from the first principles, Nano Lett. **13**, 253 (2013).

[15] D. Le and T. S. Rahman, Joined edges in $MoS_2$: Metallic and half-metallic wires, J. Phys.: Condens. Matter **25**, 312201 (2013).

[16] W. Zhou, X. Zou, S. Najmaei, Z. Liu, Y. Shi, J. Kong, J. Lou, P. M. Ajayan, B. I. Yakobson, and J.-C. Idrobo, Intrinsic structural defects in monolayer molybdenum disulfide, Nano Lett. **13**, 2615 (2013).

[17] H. Liu, L. Jiao, F. Yang, Y. Cai, X. Wu, W. Ho, C. Gao, J. Jia, N. Wang, H. Fan, W. Yao, and M. Xie, Dense network of one-dimensional midgap metallic modes in monolayer $MoSe_2$ and their spatial undulations, Phys. Rev. Lett. **113**, 066105 (2014).

[18] W. Jolie, C. Murray, P. S. Weiß, J. Hall, F. Portner, N. Atodiresei, A. V. Krasheninnikov, C. Busse, H.-P. Komsa, A. Rosch, and T. Michely, Tomonaga-Luttinger liquid in a box: Electrons confined within $MoS_2$ mirror-twin boundaries, Phys. Rev. X **9**, 011055 (2019).

[19] O. Lehtinen, H.-P. Komsa, A. Pulkin, M. B. Whitwick, M.-W. Chen, T. Lehnert, M. J. Mohn, O. V. Yazyev, A. Kis, U. Kaiser, and A. V. Krasheninnikov, Atomic scale microstructure and properties of Se-deficient two-dimensional $MoSe_2$, ACS Nano **9**, 3274 (2015).

[20] H.-P. Komsa and A. V. Krasheninnikov, Engineering the electronic properties of two-dimensional transition metal dichalcogenides by introducing mirror twin boundaries, Adv. Electron. Mater. **3**, 1600468 (2017).

[21] M. Batzill, Mirror twin grain boundaries in molybdenum dichalcogenides, J. Phys.: Condens. Matter **30**, 493001 (2018).

[22] J. Lin, S. T. Pantelides, and W. Zhou, Vacancy-induced formation and growth of inversion domains in transition-metal dichalcogenide monolayer, ACS Nano **9**, 5189 (2015).

[23] Y.-C. Lin, T. Björkman, H.-P. Komsa, P.-Y. Teng, C.-H. Yeh, F.-S. Huang, K.-H. Lin, J. Jadczak, Y.-S. Huang, P.-W. Chiu, A. V. Krasheninnikov, and K. Suenaga, Three-fold rotational defects in two-dimensional transition metal dichalcogenides, Nat. Commun. **6**, 6736 (2015).

[24] P. M. Coelho, H.-P. Komsa, H. Coy Diaz, Y. Ma, A. V. Krasheninnikov, and M. Batzill, Post-synthesis modifications of two-dimensional $MoSe_2$ or $MoTe_2$ by incorporation of excess metal atoms into the crystal structure, ACS Nano **12**, 3975 (2018).

[25] H. Zhu, Q. Wang, L. Cheng, R. Addou, J. Kim, M. J. Kim, and R. M. Wallace, Defects and surface structural stability of $MoTe_2$ under vacuum annealing, ACS Nano **11**, 11005 (2017).

[26] J. Hall, B. Pielić, C. Murray, W. Jolie, T. Wekking, C. Busse, M. Kralj, and T. Michely, Molecular beam epitaxy of quasi-freestanding transition metal disulphide monolayers on van der Waals substrates: A growth study, 2D Mater. **5**, 025005 (2018).

[27] H.-P. Komsa, J. Kotakoski, S. Kurasch, O. Lehtinen, U. Kaiser, and A. V. Krasheninnikov, Two-dimensional transition metal dichalcogenides under electron irradiation: Defect production and doping, Phys. Rev. Lett. **109**, 035503 (2012).

[28] L. Tapasztó, G. Dobrik, P. Lambin, and L. P. Biró, Tailoring the atomic structure of graphene nanoribbons by scanning

tunnelling microscope lithography, Nat. Nanotechnol. **3**, 397 (2008).

[29] Z. Pedramrazi, C. Herbig, A. Pulkin, S. Tang, M. Phillips, D. Wong, H. Ryu, M. Pizzochero, Y. Chen, F. Wang, E. J. Mele, Z.-X. Shen, S.-K. Mo, O. V. Yazyev, and M. F. Crommie, Manipulating topological domain boundaries in the single-layer quantum spin Hall insulator $1T' - WSe_2$, Nano Lett. **19**, 5634 (2019).

[30] P. Jia, W. Chen, J. Qiao, M. Zhang, X. Zheng, Z. Xue, R. Liang, C. Tian, L. He, Z. Di, and X. Wang, Programmable graphene nanobubbles with three-fold symmetric pseudo-magnetic fields, Nat. Commun. **10**, 3127 (2019).

[31] J. Lee, D. Wong, J. Velasco, Jr., J. F. Rodriguez-Nieva, S. Kahn, H.-Z. Tsai, T. Taniguchi, K. Watanabe, A. Zettl, F. Wang, L. S. Levitov, and M. F. Crommie, Imaging electrostatically confined Dirac fermions in graphene quantum dots, Nat. Phys. **12**, 1032 (2016).

[32] M.-H. Zhang, F. Gao, A. B. Lorentzen, Y.-N. Ren, R.-H. Zhang, X.-F. Zhou, R. Dong, S.-W. Gao, M. Brandbyge, and L. He, Atomic-level precision creation and manipulation of interfacial Se chemisorbates in graphene/$WSe_2$ heterostructures, Phys. Rev. B **110**, L041405 (2024).

[33] Z. Pan, W. Xiong, J. Dai, Y. Wang, T. Jian, X. Cui, J. Deng, X. Lin, Z. Cheng, Y. Bai, C. Zhu, D. Huo, G. Li, M. Feng, J. He, W. Ji, S. Yuan, F. Wu, C. Zhang, and H.-J. Gao, Ferromagnetism and correlated insulating states in monolayer $Mo_{33}Te_{56}$, arXiv:2307.06001.

[34] L. Lei, J. Dai, H. Dong, Y. Geng, F. Cao, C. Wang, R. Xu, F. Pang, Z.-X. Liu, F. Li, Z. Cheng, G. Wang, and W. Ji, Electronic Janus lattice and kagome-like bands in coloring-triangular $MoTe_2$ monolayers, Nat. Commun. **14**, 6320 (2023).

[35] See Supplemental Material at http://link.aps.org/supplemental/10.1103/PhysRevB.110.L081407 for more experimental data, analysis, and details of discussion, which includes Refs. [36–39].

[36] P. M. Coelho, H.-P. Komsa, K. Lasek, V. Kalappattil, J. Karthikeyan, M.-H. Phan, A. V. Krasheninnikov, and M. Batzill, Room-temperature ferromagnetism in $MoTe_2$ by post-growth incorporation of vanadium impurities, Adv. Electron. Mater. **5**, 1900044 (2019).

[37] Y. Zhang, M. M. Ugeda, C. Jin, S.-F. Shi, A. J. Bradley, A. Martín-Recio, H. Ryu, J. Kim, S. Tang, Y. Kim, B. Zhou, C. Hwang, Y. Chen, F. Wang, M. F. Crommie, Z. Hussain, Z.-X. Shen, and S.-K. Mo, Electronic structure, surface doping, and optical response in epitaxial $WSe_2$ thin films, Nano Lett. **16**, 2485 (2016).

[38] H. J. Liu, L. Jiao, L. Xie, F. Yang, J. L. Chen, W. K. Ho, C. L. Gao, J. F. Jia, X. D. Cui, and M. H. Xie, Molecular-beam epitaxy of monolayer and bilayer $WSe_2$: A scanning tunneling microscopy/spectroscopy study and deduction of exciton binding energy, 2D Mater. **2**, 034004 (2015).

[39] Y.-X. Zhao, X.-F. Zhou, Y. Zhang, and L. He, Oscillations of the spacing between van Hove singularities induced by sub-Ångstrom fluctuations of interlayer spacing in graphene superlattices, Phys. Rev. Lett. **127**, 266801 (2021).

[40] J. Zhang, Y. Xia, B. Wang, Y. Jin, and H. Tian, Single-layer $Mo_5Te_8$— A new polymorph of layered transition-metal chalcogenide, 2D Mater. **8**, 015006 (2020).

[41] D. Tománek and M. A. Schlüter, Calculation of magic numbers and the stability of small Si clusters, Phys. Rev. Lett. **56**, 1055 (1986).

[42] O. Echt, K. Sattler, and E. Recknagel, Magic numbers for sphere packings: Experimental verification in free xenon clusters, Phys. Rev. Lett. **47**, 1121 (1981).

[43] O. Haxel, J. H. D. Jensen, and H. E. Suess, On the "magic numbers" in nuclear structure, Phys. Rev. **75**, 1766 (1949).

[44] M. G. Mayer, On closed shells in nuclei, Phys. Rev. **74**, 235 (1948).

[45] M. G. Mayer, On closed shells in nuclei. II, Phys. Rev. **75**, 1969 (1949).

[46] J. Wang, C. F. Mbah, T. Przybilla, B. Apeleo Zubiri, E. Spiecker, M. Engel, and N. Vogel, Magic number colloidal clusters as minimum free energy structures, Nat. Commun. **9**, 5259 (2018).